JOURNAL OF MATERIALS SCIENCE 12 (1977) 2115–2123

Equations for magnetization processes based on the laws of thermodynamics

LYNN J. BRADY
P. O. Box 396, Camden, South Carolina 29020, USA

A series of logarithmic equations founded on thermodynamic principles are used to rationalize the process of magnetization. These equations yield precise power-law fits for the virgin magnetization curves of single-crystal and polycrystalline specimens. Using these equations, values of M_s are obtained without using laborious extrapolation procedures. This characteristic, together with their extreme simplicity and their ability to follow and account for the magnetization of different products over all field values, makes them very useful. These equations, their derivations and supporting data are presented in this report.

1. Introduction

It is claimed [1] that the familiar hysteresis loops of common magnets have such varied and complicated shapes that there is little hope of interpreting them by a formal theory, without introducing a large number of parameters. We shall show, however, that this number can be reduced to just a few by using a series of simple logarithmic equations in succession to follow the normal magnetization of single-crystal and polycrystalline products.

Then, we shall show that these equations yield an insight into the physical changes which take place in a specimen when it is magnetized. For example, by their means an explanation is obtained for the formation and the collapse of domains of reverse magnetization. It is apparent, therefore, that where magnetization processes are involved, they are analogous in function to the equations which are used in chemical kinetics to explain reaction mechanisms.

By means of log–log plots, based on these equations, precise values of M_s^* are obtained for materials with different crystal structures [2]. Since this is done without using the laborious extrapolation procedures required by the law of approach [3], they are very useful.

2. The displacement of domain walls

In order to derive these equations, let us consider the physical changes which take place in a specimen when it is magnetized. The specimen selected for study is comprised of polydomain crystallites. Since a crystallite's domains do not extend beyond its boundaries these domains are designated microdomains in this report.

When the specimen is placed in a weak field, one of the microdomains of a crystallite selected at random grows at the expense of the crystallite's remaining microdomains. This occurs, according to theory [4], because the domain which grows has a more favourable orientation with respect to the field than those of its neighbours.

This growth continues, as the field strength is increased in value, until the boundaries of the favoured microdomain correspond to those of the crystallite. There they are pinned, as the field strength is raised, until the critical field strength of the microdomain is reached. When this is exceeded, the walls of the microdomain snap and, thereby, form a macrodomain as illustrated by De Blois' classic example [5].

The macrodomain formed by this irreversible process obviously contains more than one crystallite within its boundaries. Hence, it can only be distinguished from a domain of reverse magnetization by the energy required to produce it. A domain of reverse magnetization, according to our theory, is formed by magnetization reversal.

When the volume of a domain changes reversibly, under constant temperature and pressure conditions, its internal energy E is changed by dE,

*M_s = saturation magnetic moment cm^{-3}.

where

$$dE = TdS - pdv, \quad (1)$$

according to the laws of thermodynamics. S is the entropy at the temperature, T(K) of a domain selected at random, v is its volume, and p is an external pressure.

The internal energy of this domain is a single-valued function of its variables. Therefore, E is expressed in terms of its components, E_m, E_k, and E_0, in the following equation:

$$E = E_m + E_k + E_0. \quad (2)$$

This is done so that equations containg these terms may be derived for the magnetization processes. The term, $E_m = -H_aM$, introduced here is the energy of magnetic interaction between H_a, the applied field, and M, the magnetization of the selected domain in the applied field direction. E_k is the energy of crystal anisotropy and E_0 is the sum of the following energy terms: E_D = the energy of shape anisotropy of the crystallite, E_σ = the energy of magnetostriction, E_e = the exchange force energy, E_N = the energy of self-demagnetization of the specimen, and E_R = all remaining energy terms we may have neglected. These energy terms, obviously, are those of a crystallite selected at random. Consequently, they are used to express its internal energy, as well as the internal energies of its microdomains on a proportional volume basis.

In order to use these energy terms, we use Gibbs' free energy function [6].

$$G = E + pv - TS, \quad (3)$$

in which G is Gibbs' free energy. The term E in this equation, is replaced by its components, $E_k + E_0 - H_aM$, from Equation 2. The resultant expression, when differentiated, yields the equation,

$$H_a dM = (dE_k + dE_0 + pdv) - (MdH_a + TdS), \quad (4)$$

after the terms, dG, dT and dp are equated to zero. This equation gives the reversible changes of magnetization permitted to take place in a crystallite, or its microdomains on a proportional volume basis, when the temperature and pressure are constant. It is obviously difficult, if not impossible, to separate the variables in this equation so that it can be solved in a straightforward manner. However, its form suggests that the empirical relationship,

$$(dE_k + dE_0 + pdv) - (MdH_a + TdS) = k_{o1}MdH_a, \quad (5)$$

may be used to obtain the approximate solution,

$$k_{o1} \ln H_a = \ln M + c_{o1} \quad (6)$$

to Equation 4. The terms, k_{o1} and c_{o1}, in this equation, are a proportionality constant and a constant of integration, respectively.

In order to establish the validity of this procedure, the magnetization of each microdomain in the specimen, as expressed by Equation 6, is multiplied by the volume of the microdomain to which it pertains. The products of this operation when summed and divided by the volume of the specimen yield the equation,

$$\ln H_a = k_1 \ln M_n, \quad (7)$$

in which k_1 is a proportionality constant and M_n is the normal magnetization of the specimen.

This equation follows the magnetization of a given specimen from $H_a = 0$ to the field at which its first macrodomain is formed. Thereafter, the equation,

$$\ln H_a = k_2 \ln M_n + c_2, \quad (8)$$

in which k_2 and c_2 are constants, is used. It follows the specimen's virgin magnetization curve over the lower half-portion generally attributed [7] to the irreversible domain wall displacement process. The precision with which Equations 7 and 8 can follow the magnetization of diverse materials is readily established. Thus, published values of H_a vs M_n from reliable sources are plotted in ln–ln form.

Equation 8 is founded on the theory that each time a microdomain wall snaps, a macrodomain is either formed or enlarged. As a result, the internal energy of the specimen jumps by ΔE as manifest by the Barkhausen [8] increase in its magnetization. Since,

$$G = E_k + E_0 + pv - H_aM - TS, \quad (9)$$

according to Equations 2 and 3, it is evident that between jumps the reversible change in magnetization of the specimen is given by the expression,

$$\Sigma H_a d\Delta M = \Sigma(d\Delta E_k + d\Delta E_0 + pd\Delta v - \Delta M dH_a - Td\Delta S), \quad (10)$$

provided the temperature and pressure are constant. Δ is used in this expression in accord with

convention [9] to indicate that the sum is taken over both micro- and macromagnetic species in this magnetization process.

Equation 10 is evaluated to a first approximation by means of Equation 6. Thus, the magnetization of each domain, as expressed by Equation 6, is multiplied by the volume of the domain to which it pertains. The products of this operation are summed and then divided by the volume of the specimen. When the specimen consists of a large assemblage of crystallites, these operations are repeated at a second field value much stronger than the first. The equations obtained are then solved simultaneously to smooth out the Barkhausen jumps. Thus, Equation 8 is obtained.

3. The rotational processes

After the specimen's microdomain walls have snapped, its magnetization vectors rotate in the applied field direction as the field strength is increased in value. Hence, the equation

$$\Sigma H_a dM = \Sigma(dE_k + dE_0 + pdv - MdH_a - TdS), \tag{11}$$

gives the changes of magnetization permitted to take place in a macrodomain selected at random. This expression, based on Equation 9, is restricted to applications where the pressure and temperature are constant and magnetization reversal is not involved. Here the sum is taken over all crystallites in the macrodomain.

According to our theory, when magnetization reversal is excluded, Equation 11 can only be applied to a macrodomain whose constituent crystallites are perfect. We propose to test this theory by means of such a specimen. Equation 11 is solved to a first approximation by means of Equation 5. Then by extending the procedure by which Equation 7 was derived so that it applies to the specimen's macrodomains, the equation

$$\ln H_a = k_3 \ln M_n + c_3, \tag{12}$$

is obtained. We use this to follow the magnetization attributed to rotation of the magnetization vectors of the specimen we shall employ whose crystallites are perfect. Then we show that the equations,

$$\ln H_a = k_4 \ln M_n + c_4, \tag{13}$$

$$\ln H_a = k_5 \ln M_n + c_5, \tag{14}$$

$$\ln H_a = k_6 \ln M_n + c_6 \tag{15}$$

are needed to follow the magnetization associated with the rotation of a specimen's magnetization vectors when its constituent crystallites are imperfect.

Equation 13 will be used at field values less than H_s, the field at which magnetization reversal becomes complete in a specimen comprised of imperfect crystallites. Therefore, according to our interpretation, it follows the specimen's magnetization curve over the upper half-portion generally attributed [7] to the irreversible domain-wall displacement process.

Following the use of Equation 13, Equations 14 and 15 are used in succession to follow the magnetization of the specimen over the range ascribed [7] to the rotation of its magnetization vectors. Thus, Equation 14 is used to follow its magnetization over the range, $H_s \leqslant H_a \leqslant H_{eff}^A$, the effective anisotropy field value, and Equation 15 is used at field values greater than H_{eff}^A.

Equations 12 to 15 are based on the process generally assumed to take place in a macrodomain selected at random. The magnetization vectors of its constituent crystallites rotate in the applied field direction as the field strength is increased in value. Consequently, the magnetization of a macrodomain increases, with increasing field strength, when the magnetization vectors of its constituent crystallites are inclined in the applied field direction. Conversely, when these vectors point away from the applied field direction, the magnetization of the macrodomain decreases with increasing field strength until it equals zero, then its magnetization vectors turn over in the field, H_{cr}, where $\Sigma H_a dM = 0$. We show, however, that at this field value

$$\Sigma(p\delta v_r - T\delta S_{conf}) = 0 \tag{16}$$

must be satisfied to comply with the laws of thermodynamics. The term, $\Sigma\delta v_r$, in this expression, is the change in the volume of the macrodomain resulting from its magnetization reversal and $\Sigma\delta S_{conf}$ is the accompanying change in its configurational entropy [10].

The configurational entropy of a crystallite depends on its perfection. Hence, the configurational entropy of a macrodomain is defined by means of the equation

$$\Sigma T\delta S_{conf} = \Sigma(\delta E_{kr} + \delta E_{or} - \delta G_r) = \Sigma T\delta S_r. \tag{17}$$

where the subscript r in this expression, denotes association with the turnover of the crystallite's magnetization vectors.

This equation is derived by summing the free energies, expressed by Equation 9, of the macrodomain's constituent crystallites. The decrement of the resultant expression yields

$$\Sigma\delta G_r = \Sigma(\delta E_{kr} + \delta E_{or} + p\delta v_r - H_a\delta M_r - M_r\delta H_a - T\delta S_r), \quad (18)$$

after the restrictions are imposed that the decrements are those of magnetization reversal and δp and δT equal zero. Since the terms, $\Sigma H_a\delta M_r$ and $\Sigma M_r\delta H_a$, must equal zero when magnetization reversal takes place, it is apparent that, by means of this equation, Equation 17 is obtained.

Equation 17 makes it evident that when the macrodomain's crystallites are perfect $\Sigma\delta S_{conf} = 0$. Therefore, when its magnetization vectors turn over, they make angles of 180° with their original directions. Moreover, they must turn over in unison to keep the macrodomain's volume constant and, thereby, satisfy Equation 16. We use Equation 12 to follow this unique magnetization process which is only exhibited by a specimen whose crystallites are perfect.

Conversely, when the crystallites are imperfect, which is the normal state [11], $\Sigma\delta S_{conf} \neq 0$, according to Equation 17. In this case, the angle of vector turn over are less than 180° and $\Sigma\delta v_r$ must be greater than zero to satisfy Equation 16. It is theorized that this change in the volume is realized when a Bloch wall sweeps through the macrodomain turning over most of its magnetization vectors. This occurs in the field, $H_a = H_{cr}$ where $\Sigma\delta M_r = 0$. The crystallites whose magnetization vectors are not turned over in this field, because occlusions and other imperfections intervene, form domains of reverse magnetization.

The near annihilation of a macrodomain in its critical field, H_{cr}, adds to the growth of its neighbours. These are oriented with the magnetic vectors of their constituent crystallites inclined in the applied field direction. It will be recognized that these processes are analogous to those expressed by means of Equation 10. Hence, by means of Equation 10 and the procedure by which Equation 8 was derived, Equation 13 is obtained.

Magnetization reversal becomes complete in the field, H_s, when the specimen's crystallites are imperfect. Thus, Equation 11 gives the reversible changes of magnetization permitted to take place in a macrodomain when $H_s \leqslant H_a \leqslant H_{eff}^A$ and the temperature and pressure are constant. In this case its terms, M, E_k, E_o, v and S are treated as extensive variables whose values change with increasing field strength. These changes are observed because a macrodomain with a favoured orientation grows at the expense of its neighbours, as the field strength is increased in value. This growth continues until the field, H_{eff}^A, is reached, where the specimen consists of a single macrodomain and its consort of domains of reverse magnetization. To follow this process Equation 14 is derived by means of Equation 6 and the procedure used to obtain Equation 8.

When H_a is made greater than H_{eff}^A, the domains of reverse magnetization become unstable [12]. Consequently, they collapse irreversibly because $\delta S_{conf} \neq 0$ and, hence, give final and complete satisfaction to Equation 16 at very high field values where $H_a \gg H_{eff}^A$. Equation 15, which follows this magnetization process, is derived by means analogous to those used to obtain Equation 13.

4. Experimental

The theories we have advanced are tested by showing that only Equations 8 and 12 are needed to follow the virgin magnetization of specimens whose constituent crystallites are single-domain and perfect. In this case, the integration constant c_2 in Equation 8 equals zero because the specimen's microdomain walls cannot move reversibly. Other tests show that Equation 8 with $c_2 = 0$, Equations 13 and 14, used in succession, are needed to follow the magnetization of a specimen, whose single-domain crystallites are imperfect, over the range $0 \leqslant H_a \leqslant H_{eff}^A$.

Additional tests show that Equations 7, 8, 13, 14 and 15 are needed to follow the magnetization of products comprised of polydomain imperfect crystallites. These tests are culminated by showing that Equations 14 and 15 yield the precise value of M_s for pure nickel without using laborious extrapolation procedures.

The specimens of single-domain crystallites required for the tests were prepared by modifying the procedure Shrik and Buessem [13] developed to make their glass products containing barium ferrites. Pure B_2O_3, $BaCO_3$, and Fe_2O_3 powders were mixed together in the following proportions by weight: 12.1, 52.9 and 34.9, respectively. This

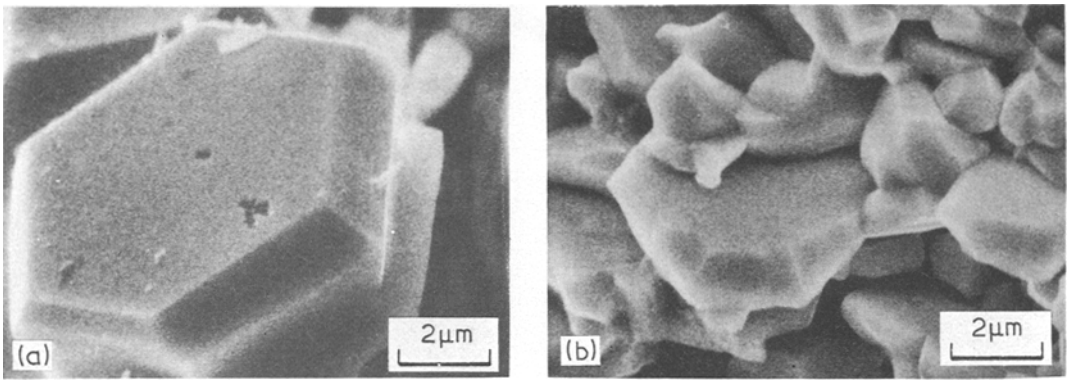

Figure 1 SEM micrographs of hexagonal barium ferrites (a) a water-leached specimen from the 1500° C melt, (b) an oriented $BaFe_{12}O_{19}$ section from a speaker magnet.

mixture was calcined to 700° C to form a friable cake, portions of which were subsequently heated to form melts which were poured at 1200° C and 1500° C, respectively. These melts were poured into water to "freeze" in their high-temperature crystal structures.

This procedure was followed because phase diagrams [14, 15] led to the conclusion that the 1200° C melt should produce specimens consisting of ferrite building blocks [15] and imperfect, single-domain, ferrite crystallites in a glass matrix. Therefore, according to our theory, Equations 8, 13, and 14, when used in succession, should follow the magnetization of specimens produced by the 1200° C melt over the range of $0 \leqslant H_a \leqslant H_{eff}^A$.

Phase diagrams [14, 15] and theories of crystal growth [11], however, lead to the conclusion that the crystallites produced by the 1500° C melt should approach perfection, and this conclusion is supported by the SEM Micrograph shown in Fig. 1. Fig. 1a is the micrograph of a water-leached specimen from the 1500° C melt. The perfection of the hexagonal crystallites produced by this melt is made apparent by comparing their micrograph with that of an oriented $BaFe_{12}O_{19}$ section from a speaker magnet shown in Fig. 1b. This perfection is also made apparent by comparing the micrograph of the water-leached specimen produced by the 1500° C melt with a micrograph of a water-leached specimen from the 1200° C melt, shown in Fig. 2.

The specimens produced by the melts are believed to have the empirical chemical formula, $Ba_2Fe_2^{2+}Fe_{12}^{3+}O_{22}$. This noteworthy conclusion is based on phase diagrams [15] and the anisotropy field value, $H^A = 28.6$ kOe, derived for the specimens produced by the 1200° C melt. This value is based on the approximation [16], $H^A \approx 2H_s$, and the term, $H_s = 14.3$ kOe, which we shall establish by means of the specimen's magnetic moments [17]. The anisotropy field value, $H^A = 28.6$ kOe, compares well with $H^A = 28.0$ kOe reported [15] for $Ba_2Co_2^{2+}Fe_{12}^{3+}O_{22}$. This comparison gives us confidence in assigning the formula, $Ba_2Fe_2^{2+}Fe_{12}^{3+}O_{22}$, to the specimens produced by the melts.

The near perfection of the crystallites produced by the 1500° C melt makes their configurational entropies approach zero. Consequently, the specimen's magnetization cannot be reversed by means of Bloch wall displacement. There is no reason to believe, however, that this perfection should interfere with the formation of macrodomains. Therefore, Equation 8, with $c_2 = 0$, and Equation 12, used in succession should follow the magnetization of the specimens produced by the 1500° C melt until magnetization reversal takes place in one of its macrodomains. This occurs at very high field values [18] when its magnetization vectors turn over in unison, according to Equation 16.

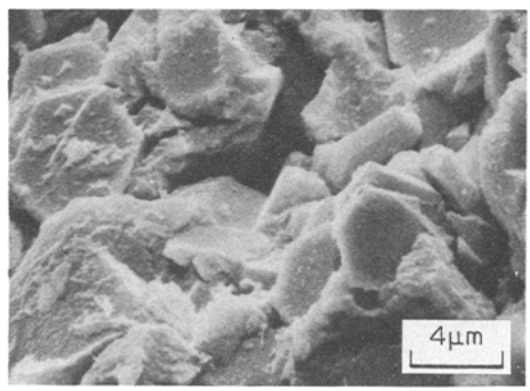

Figure 2 A SEM Micrograph of a water-leached specimen from the 1200° C melt showing the imperfect crystallites produced.

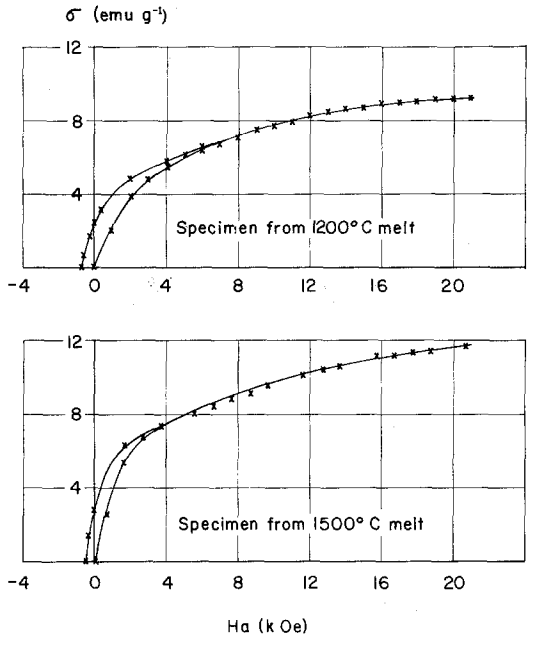

Figure 3 The virgin hystersis loops of the specimens produced by the 1200° C and 1500° C melts, respectively.

5. Results and discussion

The virgin hysteresis loops of typical specimens produced by the 1200 and 1500° C melts are shown in Fig. 3. The normal magnetic moments reported for these specimens are room-temperature values measured [17] in fields whose maximum strengths were 21 kOe. The curves shown are for specimens as-produced. Added sample preparation was avoided, since it might obscure the magnetization processes we wished to follow.

These processes are followed by means of the log–log plots of H_a versus σ_n, the normal magnetic moment per gram, presented in Fig. 4. It is seen, that the plot for the specimen produced by the 1200° C melt has three branches while that for the specimen produced by the 1500° C melt has two. In each case, the initial branch at low field values is attributed to the snapping of microdomain walls to form macrodomains and, hence, the magnetization of these specimens is followed by means of Equation 8 with $c_2 = 0$.

The second branch of the log–log plot of H_a versus σ_n for the specimen produced by the 1500° C melt is attributed to rotation of its magnetization vectors. Since magnetization reversal does not occur, this process is followed by means of Equation 12. However, the second branch of the log–log plot for the specimen produced by the 1200° C melt is attributed to the rotation of its magnetization vectors with magnetization reversal taking place by means of Bloch wall displacement. Hence, Equation 13 is used to follow this process at field values less than H_s. Equation 14 is then used to follow the magnetization of this specimen over the range, $H_s < H_a < H_{eff}^{A}$, where rotation of the magnetization vectors and growth of a macrodomain with a favoured orientation are assumed to take place.

These interpretations are shown to be reason-

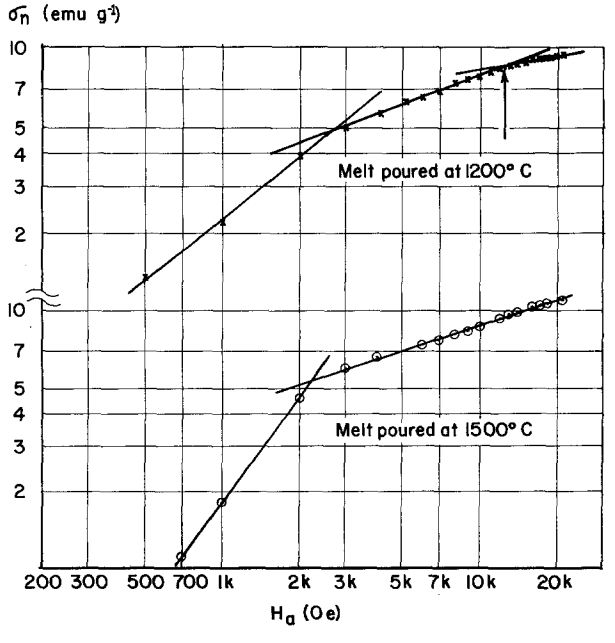

Figure 4 Log–log plots of H_a versus σ_n for the specimens whose virgin hysteresis loops appear in Fig. 3.

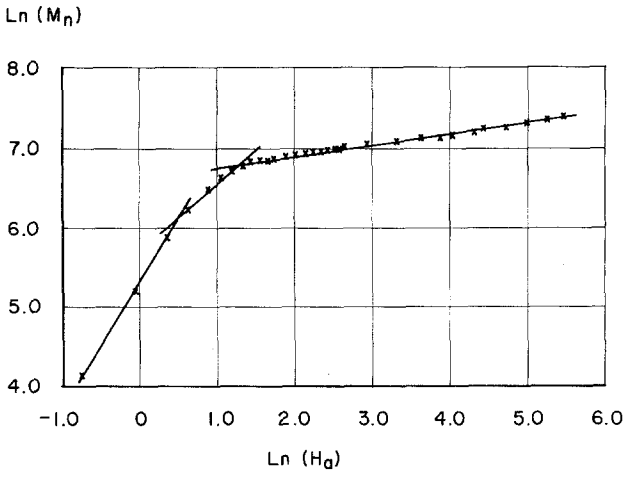

Figure 5 Ln–ln plot of H_a versus M_n for Sizoo's single-crystal iron specimen No. 1. Data from ref. (18).

able by means of Figs. 5 and 6. Thus, Fig. 5 presents a ln–ln plot of H_a versus M_n for Sizoo's [19] single-crystal iron specimen No. 1. The magnetization data for this specimen cover the range $0 < M_n < M_s$ and hence, $0 < H_a < H_s$. As a consequence, its ln–ln plot has only three branches. These are precisely followed by using Equations 7, 8 and 13 in succession.

Fig. 6, on the other hand, always displays log–log plots of H_a versus M_n which have four branches. The fifth branch required by theory does not appear because $0 < H_a < H_{eff}^A$. These log log plots, which are followed by means of Equations 7, 8 13 and 14, used in succession, are for the following products: (86II) = ferrocobalt, (149) = nickel with 0.7 wt % Mn, and (155) = malleable Heusler alloy. Data used to construct these log–log plots are from the International Critical Tables [20], which should be consulted to learn the details of specimen preparation. The arrows in this figure, as well as the one in Fig. 4, indicate the values of H_s, and it is found from Fig. 4 that $H_s = 14.3$ kOe and, hence, $H^A \approx 28.6$ kOe at room temperature for the specimens produced by the 1200° C melt. These arrows make it evident that Equations 14 and 15 have a common solution at the point, (H_s, M_n). Weiss and Forrer's data [20], for an isotropic spheroidal nickel specimen, are used to establish the value of M_n at this field value. These data are also used to show that Equation 15 is needed to follow the magnetization of a specimen at field values greater than H_{eff}^A.

In the field H_s the change in magnetization permitted to take place in each crystallite in an arbitrary specimen is expressed by the equation,

$$H_s dM - dE_N = dE_k + dE_\sigma + dE_e + dE_D + dE_R + pdv - TdS \quad (19)$$

when the temperature and pressure are constant.

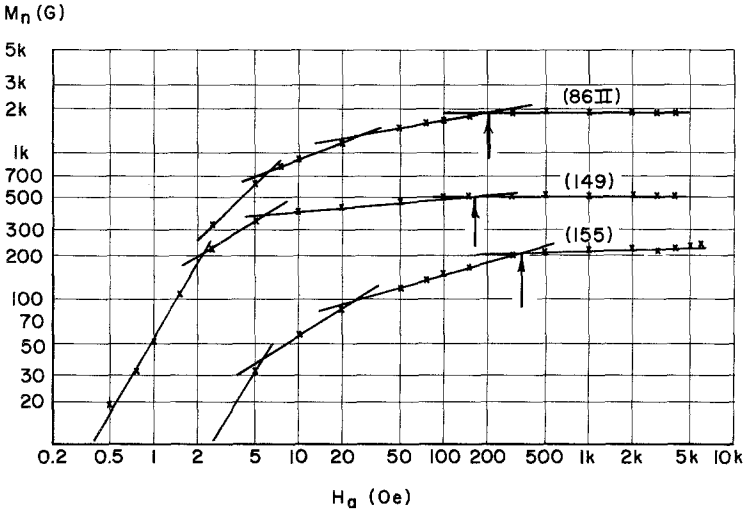

Figure 6 Log–log plot of H_a versus M_n for several products. Data from the International Critical Tables (19).

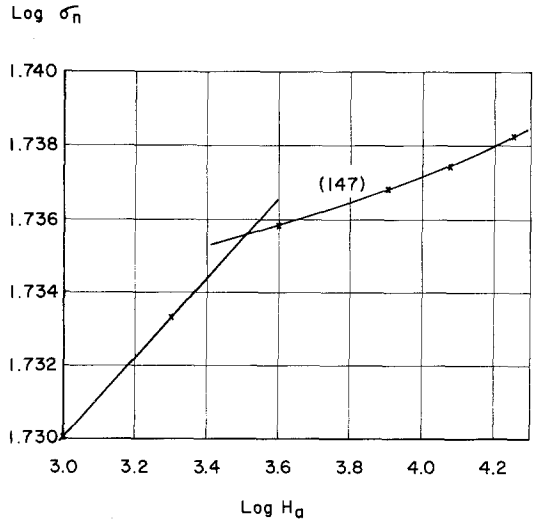

Figure 7 Log–log plot of H_a versus σ_n used to derive the value of σ_s for Weiss and Forrer's pure nickel specimen. Data from ref. (19).

At this field value, volume changes due to "forced" magnetostriction are very small [21], so that the terms pdv and dE_σ may be ignored, when seeking an approximate solution to Equation 19. It is safe to assume that the terms dE_e, dE_R, and $-TdS$ may also be neglected in solving Equation 19 to a first approximation.

The remaining terms yield the Equation [16],

$$(H^A - \bar{D}M_s) \sin 2\theta = 2(H_s - \bar{N}\bar{M}) \sin(\alpha - \theta),$$

after the required susbtitutions. The anisortopy field H^A in this expression, is approximately equal to $2K_1/M_s$, where K_1 is the first-order anisotropy constant [22]; α is the angle of inclination of a given crystallite's easy direction from the applied field direction and θ gives the angle of rotation of its magnetization vector from its rest position; $\bar{D}$ is the averaged demagnetization coefficient for the crystallite's shape anisotropy; $\bar{N}$ is the averaged self-demagnetization coefficient of the specimen and $\bar{M}$ is its averaged magnetization in the applied field direction. It is evident, therefore, that by using averaging techniques, Equation 20 can be applied to anisotropic specimens [6] as well as to those which are isotropic.

When Equation 20 is applied to an isotropic, spherical specimen, it is satisfied by means of the following values: $\bar{D} = 2\pi$, $H_s = H^A/2$ [16], $\bar{N} = 4\pi/3$ [23] $\alpha = 3\theta$, and $M = 3M_s/4$. Thus, by means of Equation 20, it is found that Equations 13 and 14 have a common solution at the point $(H_s, \bar{M}_n = \pi M_s/\bar{N})$, where $\bar{M}_n$ is the averaged value of M_n in the hard and easy directions of mangetization.

Fig. 7 demonstrates the precision with which Equations 13 and 14 yield σ_s. The data used to construct the log–log plot of H_a versus σ_n in this figure are those attributed [20] to Weiss and Forrer under the key number (147). The values of σ_n tabulated [20], are those of a spheroidal nickel specimen whose impurities and self-demagnetization have been taken into account, so that the tabulated values of H_a versus σ_n, shown in Fig. 7 in log–log, form, yield the value of σ_s directly.

Values of σ_n at field values less than 1000 Oe are not reported [20] for this specimen, so that Equations 7 and 8 cannot be used to follow its magnetization resulting from domain-wall displacement. Sufficient data are available, however, to determine by means of Fig. 7 that Equations 13

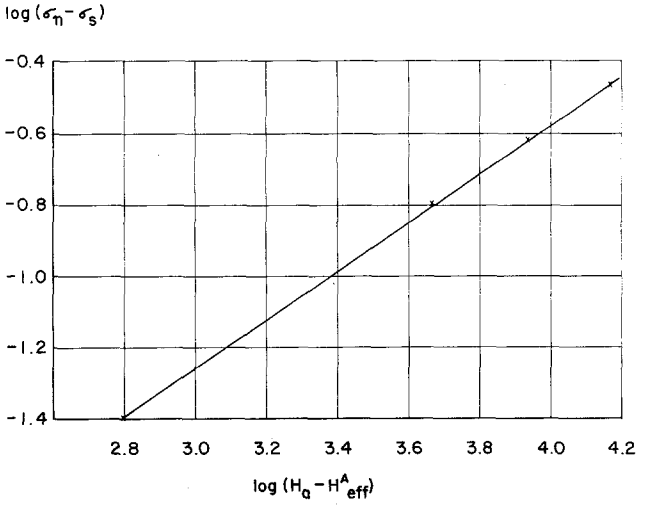

Figure 8 Log–log plot of $(H_a - H^A_{eff})$ versus $(\sigma_n - \sigma_s)$ used to show collapse of domains of reverse magnetization in fields greater than H^A_{eff}. Data from ref. [19].

and 14 have a common solution at the point, (log $H_s = 3.50650$, log $\sigma_s = 1.73555$). Thus, it is found that $H_s = 3210$ Oe and $\sigma_s = 54.39$ emu g^{-1}.

It is reported [20] that Weiss and Forrer derived the value, $\sigma_s = 54.5$ emu g^{-1}, for nickel at 18.4° C by means of extrapolation procedures and the data used to construct Fig. 7. Since the value, $\sigma_s = 54.39$ emu g^{-1}, is currently accepted [24] for nickel at 20° C, it is concluded that Equations 13 and 14 yield saturation values, within the precision limits of the measured σ_n values. This conclusion is supported by the M_s values previously derived [2] from log plots of H_a versus M_n for a number of products not considered here, including $BaFe_{12}O_{19}$ and $Sm_{1/2}Pr_{1/2}Co_5$.

In conclusion the fifth branch of the nickel log–log plot is presented in Fig. 8. This branch, which is based on Equation 15, shows that the specimen's domains of reverse magnetization collapse in fields where $H_a > H_{eff}^A = H^A - \bar{D}M_s$. Data for this plot are those of Weiss and Forrer's [20]. This plot eliminates the non-linearity observed in Fig. 7 at field values greater than H_{eff}^A. This is done by plottingl log $(H_a - H_{eff}^A)$ versus log $(\sigma_n - \sigma_s)$. Where the precision of the magnetic measurements justify the utmost rigour, the magnetic moment at H_{eff}^A should be employed instead of σ_s. but this was not justified in preparing Fig. 8. In preparing Fig. 8, the value $\bar{D} = 2\pi$ was used. In preparing was assumed that the relationship, $H^A = 2H_s$ [16] holds to a first approximation. The results seem to justify these conclusions.

Acknowledgements

I wish to thank Prof. A. E. Miller of Notre Dame University for his magnetic measurements. I am also grateful to John F. Nespor and Dennis C. Siebert of CTS Corporation for preparing the 1200 and 1500° C ferrite melts and for the SEM micrographs.

References

1. K. H. STEWART, "Ferromagnetic Domains" (Cambridge University Press, Cambridge 1954) p. 138.
2. LYNN J. BRADY, *J. Appl. Phys.* **46** (1975) 1365.
3. K. H. STEWART, "Ferromagnetic Domains" (Cambridge University Press, Cambridge 1954) p. 34.
4. R. BECKER, *Z. Physik* **62** (1930) 253; *Physik Z.* **33** (1932) 905.
5. R. W. BeBLOIS, as cited by G. D. CULLITY, "Introduction to Magnetic Materials" (Addison–Wesley, Reading, 1972) p. 308.
6. HUGH S. TAYLOR, "A Treatise on Physical Chemistry", Vol. 1, edited by Hugh S. Taylor and Samuel Glasstone (Van Nostrand, New York, 1942) p. 478.
7. RICHARD M. BOZORTH, "Ferromagnetism" (Van Nostrand, New York, 1953) p. 480.
8. H. BARKHAUSEN, *Physik. Z.* **20** (1919) 20.
9. JOHN G. ASTON, "A Treatise on Physical Chemistry" Vol 1, eidted by Hugh S. Taylor and Samuel Glasstone (Van Nostrand, New York, 1942) p. 511.
10. D. HENDERSON and H. EYRING, "Non-Stoichiometric Compounds", eidited by L. Mandelcorn (Academic Press, New York, 1964) p. 80.
11. WHEELER P. DAVEY, "A Study of Crystal Structure and its Applications" (McGraw–Hill, New York, 1934) Chapter XII.
12. J. E. DAVIES and E. A. GIESS, *J. Mater. Sci.* **10** (1975) 2156.
13. B. T. SHIRK and W. R. BUESSEM, *J. Amer. Ceram. Soc.* **53** (1970) 192.
14. H. J. VAN HOOK, "Phase Diagrams for Ceramists, 1969 Supplement", compiled by Ernest M. Levin, Carl R. Robbins, and Howard F. McMurdie, edited by Margie K. Reser (The American Ceramic Society, Columbus, 1969), Fig. 2102.
15. J. SMIT and H. P. J. WIJN, "Ferrites" (Wiley, New York, 1959) Chapter IX.
16. LYNN J. BRADY, *J. Mater. Sci.* **10** (1975) 697.
17. Measured by Professor A. E. MILLER of Notre Dame University by means of a vibrating sample magnetometer.
18. See for example C. A. FOWLER, E. M. FRYER and D. TREVES, *J. Appl. Phys.* **31** (1960) 2267.
19. G. J. SIZOO, *Z. Phys.* **56** (1929) 649.
20. "International Critical Tables", Vol. IV, edited by Edward W. Washburn (McGraw–Hill, New York, 1929) p. 360.
21. G. D. CULLITY, "Introduction to Magnetic Materials", (Addison–Wesley, Reading, 1972) p. 249.
22. J. SMIT and H. P. J. WIJN, "Ferrites" (Wiley, New York, (1959) p. 46.
23. RICHARD M. BOZORTH, "Ferromagnetism", (Van Nostrand, New York, 1953) p. 849.
24. *Idem, ibid*, p. 867.

Received 25 November 1976 and accepted 10 March 1977.